PROGRESS IN COLOR, COLORANTS AND COATINGS

available online @ www.pccc.icrc.ac.ir

Progress in Color Colorants Coating 17 (2024), 61-74

Ministry of Science, Research and Technology
Institute for Color Science & Technology

Synthesis and Corrosion Inhibition Study of 1-Aminobenzotriazole for Mild Steel in HCl Solution: Electrochemical, Surface Analysis, and Theoretical Investigations

H. Namdar-Asl[1], F. Fakheri[1], S. Pour-Ali[1,*], R. Tavangar[1], S. Hejazi[2]

[1.] Faculty of Materials Engineering, Sahand University of Technology, P.O. Box: 51335-1996, Tabriz, Iran

[2.] Faculty of Science and Technology, Chemistry and Structure of Novel Materials, University of Siegen, P.O. Box: 57076, Siegen, Germany

ARTICLE INFO

Article history:
Received: 05 June 2023
Final Revised: 31 July 2023
Accepted: 08 Aug 2023
Available online: 28 Oct 2023

Keywords:
Corrosion inhibitor
Mild steel
Drug
Electrochemical examinations
Theoretical study

ABSTRACT

The corrosion inhibition performance of a novel corrosion inhibitor, 1-aminobenzotriazole drug (1-ABT), was comprehensively evaluated through a range of experimental and computational techniques. The effectiveness of 1-ABT as a corrosion inhibitor was investigated using weight loss measurements, electrochemical methods, scanning electron microscopy (SEM), X-ray photoelectron spectroscopy (XPS), and quantum chemical/molecular dynamics studies. Experimental findings revealed a positive relationship between the inhibition effectiveness of 1-ABT and its concentration, while displaying a negative correlation with temperature. Notably, the highest achieved inhibition efficiency of approximately 98 % was observed at a concentration of 400 ppm. The adsorption behavior of 1-ABT on the metal surface was found to conform to the Langmuir adsorption isotherm, indicating monolayer formation. The thermodynamic analysis further supported the physiochemisorption nature of the adsorption process. XPS analysis and theoretical investigations confirmed the adsorption of 1-ABT molecules onto the steel surface, with the interaction between the N atoms of 1-ABT and the vacant d-orbitals of Fe atoms playing a significant role. SEM examinations provided additional evidence, demonstrating a notable reduction in the corrosion rate in the presence of 1-ABT. These findings contribute to the understanding of the corrosion inhibition mechanisms and highlight the potential of 1-ABT as an effective inhibitor for mitigating corrosion in various applications. Prog. Color Colorants Coat. 17 (2024), 61-74© Institute for Color Science and Technology.

1. Introduction

Mild steel (MS) plays a key role in the human life due to its low price, excellent toughness, high mechanical strength, good fatigue strength, ideal weldability, and enhanced availability. This material inevitably comes into contact with acidic media in various applications, such as oil-well acidizing, acid pickling, and descaling. In acidization of oil-wells, HCl is forced into the oil-well to increase the oil production [1-3]. In acid pickling, hydrochloric acid (HCl) is typically employed to remove the surface oxides remained from annealing and forging treatments. Descaling is generally carried out through the diluted HCl solutions to prepare the MS surface for the surface engineering. In all of these mentioned conditions, the reaction between MS and HCl solutions may lead to severe corrosion, resulting significant direct and indirect costs [4-6]. Therefore, it is necessary to find efficient methods to prevent,

*Corresponding author: * pourali@sut.ac.ir
Doi: 10.30509/pccc.2023.167145.1224

control, or mitigate this issue.

The application of different coatings, the use of alloying elements such as Cr, cathodic protection, and corrosion inhibitors (CIs) are among the most common methods for preventing and controlling MS corrosion in HCl media [7-11]. Among these methods, the addition of CIs is a low-cost and simple operation that is widely used to mitigate the corrosion rate of MS. These materials are added in small quantities to corrosive solutions and are physically or chemically adsorbed onto the MS surface [12, 13]. As a result, a film forms on the surface of MS, significantly decreases the corrosion rate. Dependent upon the nature of CIs, they can be categorized into two groups: inorganic and organic [14]. Chromates and nitrates are among the most efficient inorganic CIs which are toxic and harmful to the human health and environment. On the other hand, organic CIs are typically characterized by heteroatoms (namely, N, O, and S) with a pair of non-bonding electrons, double or triple bonds, and/or aromatic rings. These features determine their adsorption mechanism on the surface of MS [15-17]. A wide range of CIs have been introduced for the corrosion of MS in HCl [14, 18-22]. However, the development and introduction of new non-toxic CIs with high efficiency remains of great importance. It aims to improve corrosion protection, address environmental concerns, achieve cost-effectiveness, gain insights into the underlying mechanisms, and expand the range of available inhibitor choices.

Given the chemical formula and molecular structure of the drugs, these materials have been recently introduced as efficient CIs for MS in HCl solutions [3, 22-24]. Shojaee et al. [25] investigated the inhibition effect of Tetracycline drug on MS in 1 M HCl. They reported that the maximum inhibition efficiency (*IE*) is around 82 % with 300 ppm of Tetracycline. Kannan et al. [26] studied the *IE* of Antipsychotic drug in HCl solution. Based on their findings, using only 100 ppm of Antipsychotic may result in an *IE* of 98.8 %. By using a series of electrochemical techniques, Zakaria et al. [27] showed that 1200 ppm of Herbal drug leads to an *IE* of 97.5 %. The *IE* of other drugs, such as cefotaxime sodium, cefixime, ceftriaxone, ciprofloxacin, amoxicillin, phenothiazine, metformin, tramadol, pioglitazone, cysteine, cephapirin, tenoxicam, tiazofurin, and cefalexin has also been studied in HCl environment [28–30].

Considering the recent advances in the use of pharmaceutical compounds as effective CIs for MS in HCl solutions, it is important to explore new options in this field. In line with these investigations, this study focuses on evaluating the *IE* of 1-aminobenzotriazole (1-ABT), a novel and non-toxic corrosion inhibitor, for MS in HCl solution. To accomplish this, a comprehensive approach involving weight loss measurements, electrochemical examinations, field-emission scanning electron microscopy (FE-SEM), and X-ray photoelectron spectroscopy (XPS) is employed. Furthermore, the obtained experimental results are validated through quantum chemical and molecular dynamic simulations, providing a comprehensive understanding of the inhibitory mechanism of 1-ABT on MS corrosion in HCl solution.

2. Experimental

2.1. Materials

MS Plates with dimensions of 10×10×3 mm^3 and a chemical composition mentioned in Table 1 were used as the studied material. To prepare the samples for weight loss and electrochemical measurements, a polishing procedure was conducted up to #1000 emery paper. Subsequently, all samples underwent a cleaning process involving sequential steps: washing in distilled water (DW), sonication in ethanol for 60 seconds, and drying using warm air. It is noteworthy to mention that the necessary chemicals for both the synthesis of 1-ABT and the preparation of corrosive media were provided by the Merck Company. The synthesis protocol for 1-ABT followed the methodology outlined in reference [31]. Figure 1 displays the molecular structure of 1-ABT. The chemical structure of 1-ABT was analyzed using the Nicolet™ iS50 Fourier transform infrared (FTIR) spectrometer in the wavenumber range of 4000-400 cm^{-1}.

Table 1: Chemical composition of MS samples.

C	Si	Mn	S	P	Cr	Fe
0.18	0.12	0.41	0.01	0.01	0.10	Bal.

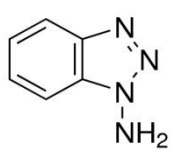

Figure 1: The molecular structure of 1-ABT molecule.

2.2.Weight loss method

The determination of weight loss was conducted by measuring the initial weight of the cleaned and dried MS samples using a precision scale with an accuracy of 10 µg. Subsequently, the MS samples were immersed in varying concentrations (0, 100, 200, 300, and 400 ppm) of the 1-ABT drug dissolved in a 0.5 M HCl solution for a duration of 100 hours. After immersion, the samples were washed with distilled water, dried, and weighed again. The inhibition performance (IE_G) and surface coverage (θ_G) parameters were then calculated using the following formulas for each experimental condition (Eqs. 1 and 2) [32]:

$$IE_G = \frac{w_0 - w_1}{w_0} \times 100 \quad (1)$$

$$\theta_G = \frac{w_0 - w_1}{w_0} \quad (2)$$

The subscript of G indicates the gravimetric method. The weight loss values of coupons in the absence (w_0) and presence (w_1) of 1-ABT were recorded. To determine the corrosion rate in mils penetration per year (mpy), Eq. 3 was employed [33].

$$corrosion\ rate = 534\frac{W}{DAT} \quad (3)$$

In Eq. 3 the variables W and D respectively denote the weight loss (mg) and density (g/cm^3) of the MS material. Furthermore, the variable A signifies the exposed area of the MS coupons (in^2), while T represents the duration of immersion (h).

2.3. Electrochemical measurements

A potentiostatic device (ZAHNER IM6x) was used to perform electrochemical tests. To establish the conventional three-electrode cell, the MS samples served as the working electrode, Ag/AgCl functioned as the reference electrode, and a platinum electrode with a surface area of 1 cm^2 was utilized as the counter electrode. Two sets of experiments were performed in a manner similar to the weight loss measurements. The first set involved varying concentrations of 1-ABT (100, 200, 300, and 400 ppm), while the second set was conducted without the presence of 1-ABT, using 0.5 M HCl as the corrosion solution. The open circuit potential (OCP) was recorded for 60 minutes before each electrochemical test to reach a stable state at the solution/working electrode interface. Potentiodynamic polarization (PDP) studies were performed by scanning the electrode potential in the range of -800 to -200 mV with respect to Ag/AgCl using a scanning speed of 1 mV/s at approximately 30°C. PDP parameters, including i_{corr} (corrosion current density), E_{corr} (corrosion potential), β_a (anodic Tafel slope) and β_c (cathodic Tafel slope), were measured using the Tafel extrapolation method [34]. In addition, IE_P and θ_P values were calculated using the following equations (Eqs. 4 and 5).

$$IE_P = \frac{i_{corr}^{blank} - i_{corr}^{with\ inhibitor}}{i_{corr}^{blank}} \times 100 \quad (4)$$

$$\theta_P = \frac{i_{corr}^{blank} - i_{corr}^{with\ inhibitor}}{i_{corr}^{blank}} \quad (5)$$

At the optimal concentration of 1-ABT, PDP tests were conducted at various temperatures (40, 50, and 60 °C) to determine the adsorption mechanism of 1-ABT. Additionally, electrochemical impedance spectroscopy (EIS) was employed in the frequency range of 100 kHz to 10 mHz with an amplitude voltage of 10 mV. Finally, the EIS data were modeled using ZView softaware.

2.4. Quantum chemical and molecular dynamics studies

The quantum chemical studies and molecular dynamics (MD) simulations were performed using Material Studio 5.0 software. For geometry optimization and the calculation of quantum chemical parameters, such as the energy of the highest occupied molecular orbital (E_{HOMO}), the energy of the lowest unoccupied molecular orbital (E_{LUMO}), the energy gap (ΔE=E_{LUMO}-E_{HOMO}), hardness (η), absolute electronegativity (χ), the fraction of transferred electrons (ΔN), and dipole moment (µ in Debye), the DMol3 module with a basis set comprising double numerical plus d-functions (DND) was employed. The values of χ, η, and ΔN were calculated using Eqs. 6-8 [35, 36].

$$\chi = -\frac{(E_{HOMO} + E_{LUMO})}{2} \quad (6)$$

$$\eta = -\frac{(E_{HOMO} - E_{LUMO})}{2} \quad (7)$$

$$\Delta N = \frac{\chi_{Fe} - \chi_{inhibitor}}{2(\eta_{Fe} + \eta_{inhibitor})} \quad (8)$$

The values of χ_{Fe} and η_{Fe} are 7 and 0 eV/mol, respectively. The MD simulations were conducted to assess the stable adsorption configuration and binding energy of 1-ABT molecule on the Fe (1 1 0) surface. The calculations were optimized using the COMPASS II force field, and the simulations were carried out for a duration of 500 ps with a time step of 1.0 fs using the NVT ensemble at a temperature of 298 K. The binding energy between the CIs and the Fe (1 1 0) surface was determined using Eq. 9, as reported by Kaya et al. [37].

$$E_{binding} = -E_{adsorption} = -(E_{total} - (E_{substrate} + E_{inhibitor})) \quad (9)$$

where $E_{binding}$ and $E_{adsorption}$ are the binding energy and adsorption energy of each inhibitor, respectively. Additionally, E_{total}, $E_{substrate}$, and $E_{inhibitor}$ are the total energy of the simulation, the energy of Fe (1 1 0) substrate together with the H_2O molecules, and the energy of inhibitor, respectively.

$E_{binding}$ refers to the binding energy of inhibitor, while $E_{adsorption}$ represents the adsorption energy. Furthermore, E_{total}, $E_{substrate}$, and $E_{inhibitor}$ correspond to the total energy of the simulation, the energy of the Fe (1 1 0) substrate, and the energy of the inhibitor, respectively

2.5. Surface characterization

The surface characteristics of MS coupons were investigated after immersion in uninhibited (0.5 M HCl) and inhibited (0.5 M HCl + optimized concentration of 1-ABT) solutions for a duration of 100 hours at approximately 30 °C. Surface morphology analysis was conducted using a field-emission scanning electron microscope (FE-SEM, MIRA3 TESCAN). Furthermore, the investigation of 1-ABT adsorption was accomplished by recording high-resolution spectra of N 1s using X-ray photoelectron spectroscopy (XPS) with a PHI 5000 VersaProbe instrument produced by Ulvac-PHI. The CASA XPS software was employed to determine the binding energy associated with N 1s peak, using Gaussian-Lorentzian lines and the Shirley background type. The energy scale calibration was performed by adjusting the C 1s peak at 284.82 eV.

3. Results and Discussion

3.1. FTIR analysis

The FTIR analysis provides valuable information about molecular vibrations, aiding in the identification of characteristic chemical bonds and groups present in the synthesized 1-ABT. Figure 2 depicts the FTIR spectrum of 1-ABT. A strong adsorption peak at 2815 cm^{-1} is observed, which can be attributed to the stretching vibrations of C-H bonds in the aromatic ring. This peak is typical of aromatic compounds and confirms the presence of the benzene ring in 1-ABT. A peak at 1293 cm^{-1} suggests the presence of stretching vibrations of C-N bonds, characteristic of the amine functional group in 1-ABT. Another peaks at 1204 cm^{-1} and 1085 cm^{-1} further support the existence of C-N stretching vibrations, confirming the presence of amines in the molecular structure. The appearance of a peak at 1017 cm^{-1} can be attributed to the bending vibrations of C-H bonds in the aromatic ring. Moreover, the presence of peaks at 821 and 678 cm^{-1} suggesting the out-of-plane bending and in-plane bending vibrations of the triazole ring, respectively. Lastly, a peak at 522 cm^{-1} indicates the wagging vibrations of C-N bonds, further supporting the presence of the amine functional group in the molecule. The observed peak values closely align with the reported data in references [38-40].

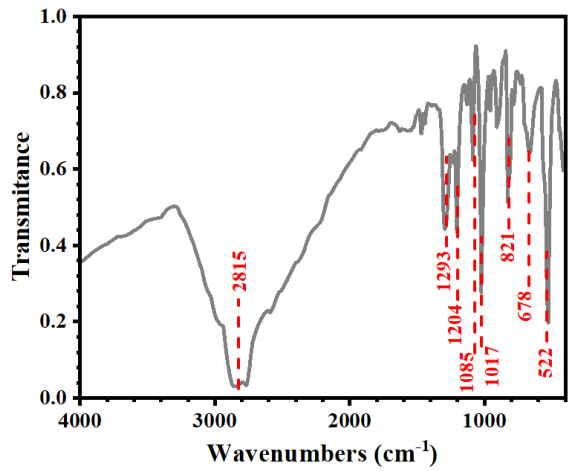

Figure 2: FTIR spectrum of the synthesized 1-ABT.

3.2. Weight loss measurements

Table 2 presents the data obtained from weight loss calculations following a 100-hour immersion of MS specimens in a 0.5 M HCl solution with varying concentrations of 1-ABT. The results reveal an increase in the IE_G values from ~81 to ~98 % as the concentration of 1-ABT rises from 0 ppm to 400 ppm. This indicates that 1-ABT demonstrates significant effectiveness as a corrosion inhibitor for MS in HCl solutions, with its inhibitory capabilities improving alongside its concentration. Moreover, the non-linear relationship between IE_G values and 1-ABT concentration suggests that once a saturation adsorption point is reached (as observed with 400 ppm of 1-ABT), the adsorption capacity remains relatively unchanged, indicating that higher concentrations of 1-ABT do not provide significant additional efficiency.

3.3. OCP measurements

Figure 3 illustrates the variation of OCP values in different test solutions. The OCP in the blank solution demonstrates a noticeable shift towards more negative values, indicating the dissolution of surface films prior to reaching a stable state. Approximately 17 minutes into the experiment, its OCP stabilizes at a constant value of -480 mV vs. Ag/AgCl. Solutions containing 1-ABT show a similar initial reduction in OCP, although the effect diminishes as the concentration of 1-ABT increases. As the concentration of 1-ABT rises, the OCP values display an increase towards more noble values. Specifically, the inhibited solution containing 400 ppm 1-ABT demonstrates the highest OCP value at -434 mV vs. Ag/AgCl. This change in OCP potentially signifies the adsorption of 1-ABT molecules and the development of a protective film on the MS surface [41, 42]. Subsequently, the OCP values for all samples remain relatively constant after 50 minutes. Consequently, all electrochemical tests were conducted following a 60-minute immersion in the corresponding solution.

3.4. PDP measurements

In order to gain a more comprehensive understanding of the kinetics involved in cathodic and anodic reactions, PDP examinations were conducted. Figure 4 presents the polarization curves of MS electrodes immersed in 0.5 M HCl solutions containing varying concentrations of 1-ABT (0, 100, 200, 300, and 400 ppm).

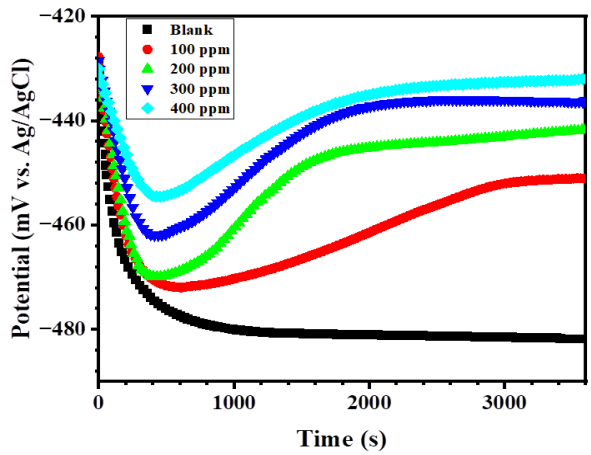

Figure 3: Variation of OCP versus immersion time for different test solutions.

Table 2: The weight loss data obtained from immersion of MS samples in uninhibited and inhibited solution.

Concentration (ppm)	Initial weight (g)	Final weight (g)	Weight loss (mg)	Corrosion rate (mpy)	*IEG%*	*θ*
Blank	2.15372	2.05812	95.6	1759.38	-	-
100	2.13541	2.11791	17.5	322.06	82	0.82
200	2.14498	2.13558	9.4	172.99	90	0.90
300	2.14369	2.13899	4.7	86.49	95	0.95
400	2.14093	2.13883	2.1	38.64	98	0.98

Table 3: The PDP parameters for the MS samples immersed in different test solutions.

Concentration (ppm)	E_{corr} (mV vs. Ag/AgCl)	i_{corr} (μA/cm^2)	$-\beta_c$ (mV/decade)	β_a (mV/decade)	IE_P%	θ
Blank	-459	311	92	90	-	-
100	-418	58	81	68	81	0.81
200	-408	35	66	63	89	0.89
300	-413	16	68	54	95	0.95
400	-428	7	69	53	98	0.98

Table 3 provides the corresponding values for E_{corr}, i_{corr}, β_c, β_a, IE_P, and θ_P. Similar to the results obtained from gravimetric analyses, the addition of 1-ABT has significantly reduced the corrosion rate of MS coupons. As depicted in Figure 4, both anodic and cathodic current densities display a decrease as the concentration of 1-ABT increases. This reduction in current density can be attributed to the adsorption of 1-ABT molecules on the surface of MS, which subsequently blocks active sites and hinders the corrosion process [43]. The data provided in Table 3 indicates that as the concentration of 1-ABT increases, both the anodic and cathodic Tafel slopes decrease. This observation implies that electrochemical reactions are facilitated by a higher absorption of 1-ABT. The interaction between inhibitor molecules and iron atoms, leading to electron sharing, is responsible for lowering the activation energy barrier for iron dissolution. Consequently, this phenomenon contributes to the enhanced ease of electrochemical reactions in the presence of higher levels of 1-ABT absorption [44].

Furthermore, the introduction of 1-ABT leads to a shift in the corrosion potential towards the anodic region. However, this shift is not substantial enough to classify it as an anodic inhibitor. Corrosion inhibitors can be categorized as anodic, cathodic, or mixed-type based on the extent of potential shifting. Anodic inhibitors are identified when the potential shift exceeds +85 mV, while cathodic inhibitors are determined when the shift exceeds -85 mV. Otherwise, if the potential shift falls within these ranges, it is considered a mixed-type corrosion inhibitor. The maximum corrosion potential shift achieved with 1-ABT is +41 mV, observed at a concentration of 400 ppm. Therefore, based on this evaluation, 1-ABT is classified as a mixed-type corrosion inhibitor.

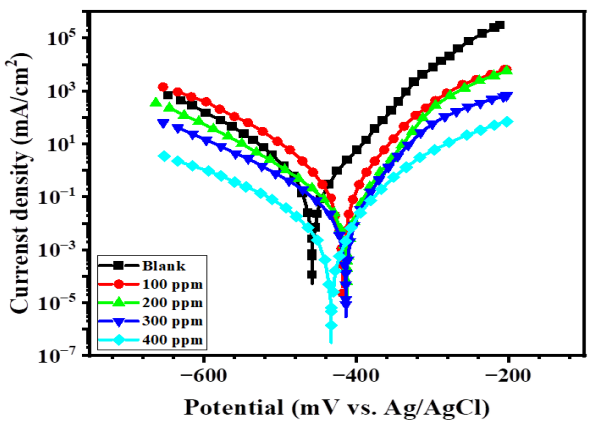

Figure 4: PDP curves for various test solutions.

3.5. Effect of temperature

The influence of temperature on the interaction between the inhibitor-containing acid and the metal is intricate due to numerous surface changes that take place, including desorption, decomposition, and rearrangement of the inhibitor [45]. In fact, different temperatures have the potential to impact the corrosion rate of MS in HCl solution both in the absence and presence of the optimal inhibitor concentration. To investigate this, PDP tests were conducted within a temperature range of 30-60 ºC for solutions without inhibitors and solutions containing the inhibitor at the optimal concentration of 400 ppm. The objective was to examine the effect of temperature on the corrosion rate of MS and the inhibition efficacy of 1-ABT. Table 4 displays the i_{corr}, E_{corr}, and IE_G values obtained from immersing the MS samples at different temperatures. The results indicate a direct correlation between the corrosion rate and temperature increase, with higher temperatures diminishing the inhibitory effect. This rise in corrosion rate can be attributed to desorption and decomposition mechanisms of inhibitor molecules [32].

Table 4: The PDP parameters assessed at various temperatures for MS immersed in the blank solution and in the inhibited solution containing 400 ppm of 1-ABT.

T (°C)	Blank		Inhibited solution		
	E_{corr} (mV)	i_{corr} (µA/cm^2)	E_{corr} (mV)	i_{corr} (µA/cm^2)	IE_P%
30	-459	378.1	-428	7.1	98
40	-472	1275.4	-467	105.4	92
50	-491	1913.7	-477	402.1	79
60	-508	2729.5	-492	734.5	73

To gain a better understanding of the impact of temperature on the activation energy of the corrosion process, the Arrhenius equation (Eq. 10) was employed.

$$\ln(i_{corr}) = \ln A - \frac{E_a}{RT} \quad (10)$$

where A denotes the Arrhenius pre-exponential factor, T represents the absolute temperature, R symbolizes the gas constant, and E_a represents the activation energy. Figure 5 illustrates the relationship between $\ln(i_{corr})$ and $1/T$, obtained through linear regression analysis. From this plot, the value of E_a can be derived using Eq. 10. According to Figure 4, the plot of the solution containing the inhibitor exhibits a steeper slope compared to the plot of the solution without the inhibitor, indicating higher activation energy and a greater energy barrier for the corrosion process, i.e., the adsorption of 1-ABT molecules onto the MS surface. The activation energy value for the solution without the inhibitor is approximately 53 kJ/mol, while for the solution containing 400 ppm 1-ABT, it is approximately 127 kJ/mol.

3.6. Adsorption characteristics

The typical mechanism involved in the adsorption of inhibitor molecules is a process known as substitutional adsorption, where there is an exchange of molecules between those adsorbed on the surface and the inhibitor molecules present in the solution (Eq. 11) [34].

$$Org(sol) + nH_2O(ads) \rightarrow Org(ads) + nH_2O(sol) \quad (11)$$

where Org(sol) is dissolved inhibitors, H_2O(ads) is absorbed water molecules, Org(ads) is absorbed inhibitors, H_2O(sol) is dissolved water molecules, and n is the replacement ratio of water molecules with an inhibitor molecule. The adsorption isotherm adheres to the principles of the Langmuir theory. Using this framework, the correlation between surface coverage (θ) and inhibitor concentration (C) is examined based on the following equation (Eq. 12) [3].

$$\frac{C}{\theta} = \frac{1}{K_{ads}} + C \quad (12)$$

where K_{ads} is the equilibrium constant for the adsorption reaction. The observed graph in Figure 6 displays a slope that approaches 1, and the high correlation coefficient ($R^2 > 0.99$) provides confirmation of conformity with the Langmuir adsorption isotherm. As per the Langmuir isotherm, it is postulated that the adsorbed molecules exclusively occupy a single site and do not interact with other adsorbed species [46].

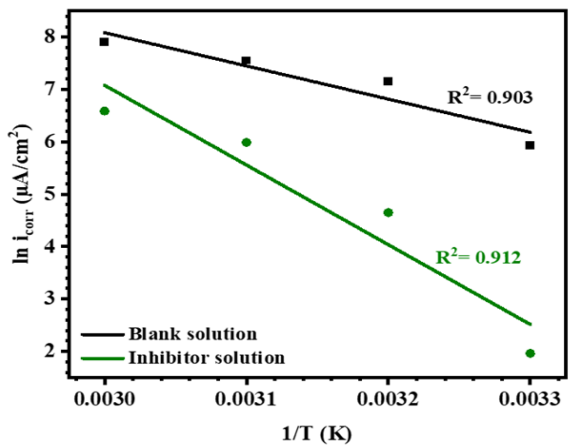

Figure 5: Ln i_{corr} vs. 1/T for MS samples immersed in the blank (0.5 M HCl) and inhibited (0.5 M HCl + 400 ppm) solutions.

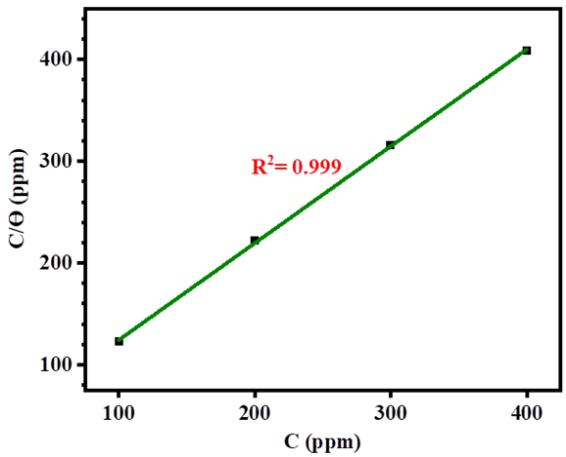

Figure 6: Adsorption behavior of 1-ABT in 0.5 M HCl: Langmuir adsorption isotherm analysis.

The value of K_{ads} is equal to the inverse of the intercept. The relationship between K_{ads} and the standard adsorption-free energy ($\Delta G°_{ads}$) is obtained from Eq. 13 [47].

$$\Delta G^{\circ}_{ads} = -RT \ln(10^6 K_{ads}) \quad (13)$$

In Eq. 13, R is the gas constant, T is the absolute temperature, and 10^6 is the mass concentration of water in the solution. For the 1-ABT inhibitor, the estimated value of $\Delta G°_{ads}$ is approximately -26.78 kJ/mol. The negative sign of $\Delta G°_{ads}$ indicates the spontaneous nature of the inhibitor adsorption reaction on the metal surface and the favorable stability of the formed layer. Generally, values above -20 kJ/mol suggest the occurrence of physical adsorption, involving electrostatic interactions between the inhibitor molecules and the metal surface. Conversely, values below -40 kJ/mol indicate chemical adsorption, where electrons are shared between the inhibitor and the MS surface, forming covalent bonds. Values between -20 kJ/mol and -40 kJ/mol signify a combination of both adsorption mechanisms [47]. Therefore, the adsorption of 1-ABT on the surface of the MS sample in a 0.5 M HCl solution can be characterized as a combination of physiochemisorption, involving both physical and chemical adsorption processes.

3.7. EIS examination

Figure 7 exhibits the Nyquist, Bode modulus, and Bode phase plots of the MS samples immersed in different test solutions at ambient temperature. The overall analysis of the EIS data reveals the presence of a single semicircular arc in the Nyquist plot and a corresponding peak in the Bode-phase plot. These observations indicate the dominance of a specific electrochemical process characterized by a single characteristic time constant. The Nyquist plot (Figure 7a) reveals that the semicircle diameter of the solution containing the inhibitor is significantly larger than that of the blank solution. Furthermore, as the inhibitor concentration increases, the corresponding semicircle diameter also increases, indicating a substantial enhancement in both polarization resistance and the inhibition efficiency of 1-ABT. The Bode modulus plot (Figure 7b) demonstrates an increase in the low-frequency impedance modulus with higher concentrations of 1-ABT. Moreover, in Figure 7c, the MS sample immersed in the solution containing 400 ppm 1-ABT demonstrates the highest phase angle, thereby confirming its superior inhibition efficiency. Randle's equivalent circuit, depicted in Figure 7d, was utilized to model the EIS data. Table 5 presents the corresponding fitting parameters. The circuit comprises three components: CPE_{dl}, which represents the constant phase element of the double layer, R_s, the solution resistance, and R_p, the polarization resistance. The value of CPE_{dl} is obtained from the following equation (Eq. 14).

$$C_{dl} = P^{1/n} R_P^{(1-n)/n} \quad (14)$$

In Eq. 14, C_{dl} represents the capacitance of the double layer, P denotes the magnitude of the constant phase element (CPE), and n represents the deviation parameter. According to Table 5, the R_P values exhibit an increase with rising inhibitor concentration. As the concentration of the corrosion inhibitor increases, there is a corresponding increase in the number of inhibitor molecules available for adsorption on the metal surface. The adsorption of the corrosion inhibitor molecules on the metal surface forms a protective physical barrier, impeding the access of corrosive species, such as chloride ions or aggressive molecules, to the metal surface. This barrier effectively reduces the rate of anodic reactions occurring at the metal-electrolyte interface, leading to an increase in the polarization resistance. Additionally, the reduction in C_{dl} may be attributed to factors such as an increase in the double layer thickness, a decrease in the dielectric constant, and a decrease in the metal's dissolution rate. The increase in the value of n with increasing the concentration of 1-ABT also signifies an improvement in the surface homogeneity of the MS due to the adsorption of the inhibitor [46, 48].

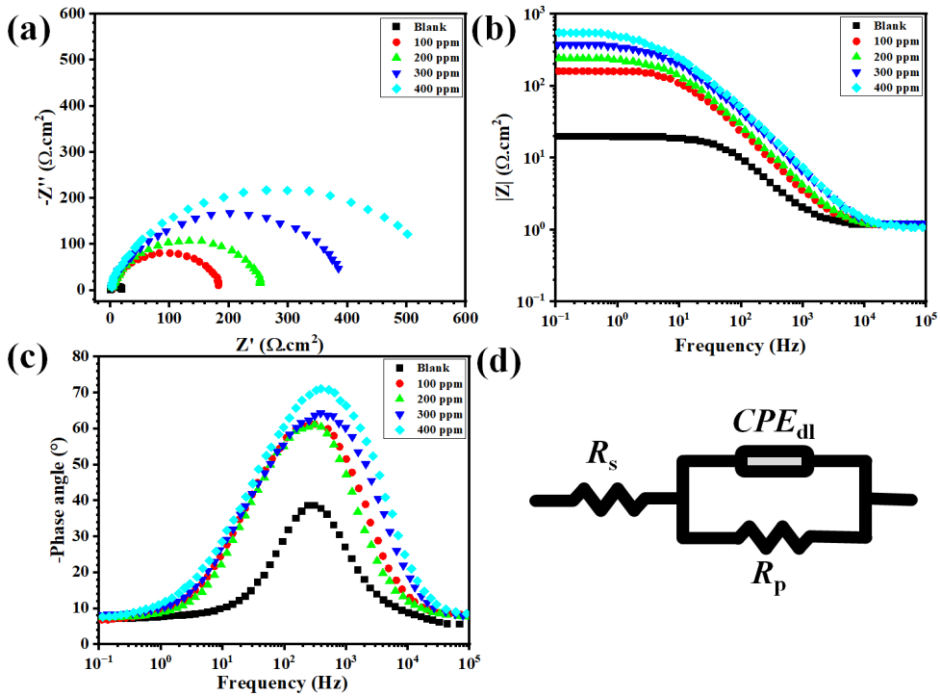

Figure 7: The results of EIS for various test solutions: (a) Nyquist, (b) Bode-Modulus, and (c) Bode-phase plots. (d) Equivalent circuit used to model the EIS data.

Table 5: EIS data for MS samples in 0.5 M HCl solution containing different concentrations of 1-ABT.

Concentration (ppm)	R_s (ohm.cm^2)	R_p (ohm.cm^2)	CPE_{dl}		C_{dl} (μF/cm^2)
			P (μF/cm^2)	n	
Blank	0.5	15	577	0.91	1414.4
100	1.5	194	149	0.91	411.5
200	1.8	269	102	0.92	248.0
300	2.0	324	89	0.94	171.4
400	2.2	362	84	0.95	144.6

3.8. Surface characterizations

The images in Figure 8 illustrate the surface characteristics of MS samples after being immersed in different solutions: the blank solution and solutions containing inhibitor (0.5 M HCl + 400 ppm of 1-ABT) for a duration of 100 h. Figure 8a demonstrates that the unexposed sample exhibits a uniform and smooth surface with some typical micro-scratches resulting from the grinding process. In contrast, when the same surface is exposed to a 0.5 M HCl solution without an inhibitor, it undergoes severe corrosion, leading to the complete coverage of the surface by corrosion products. This results in a significantly roughened surface on a microscopic scale, as depicted in Figure 8b. However, in the case of the inhibited solution, although no evidence of lines resulting from initial grinding is observed, the level of surface roughness due to corrosion is lower compared to the uninhibited solution. Additionally, a few localized signs of corrosion attack are observed (Figure 8c). Figure 9 illustrates the high-resolution N 1s spectra for the MS samples after being immersed in both the blank solution and the inhibited solution (0.5 M HCl + 400 ppm of 1-ABT) for 100 hours. It is worth noting that the MS coupons do not contain nitrogen, while 1-ABT does. Therefore, the absorption of 1-ABT molecules can be examined by analyzing the high-resolution N 1s peak.

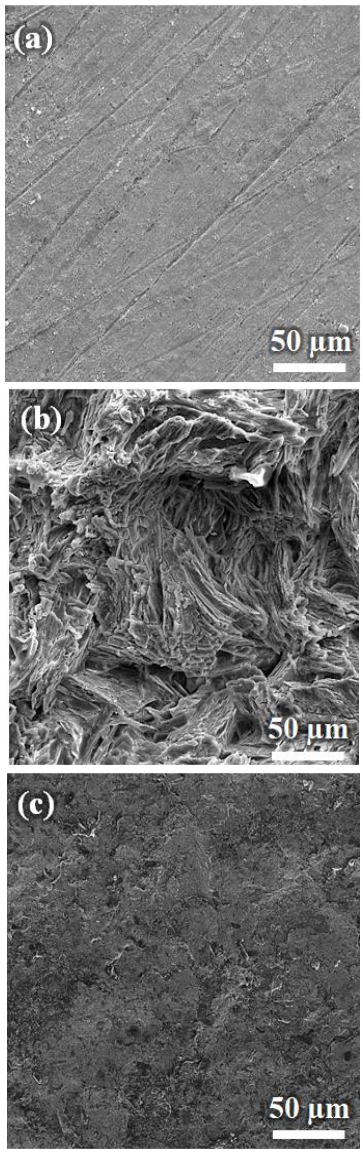

Figure 8: SEM examinations of MS coupons: (a) before immersion, (b) after immersion in 0.5 M HCl, and (c) after immersion in 0.5 M HCl + 400 ppm 1-ABT.

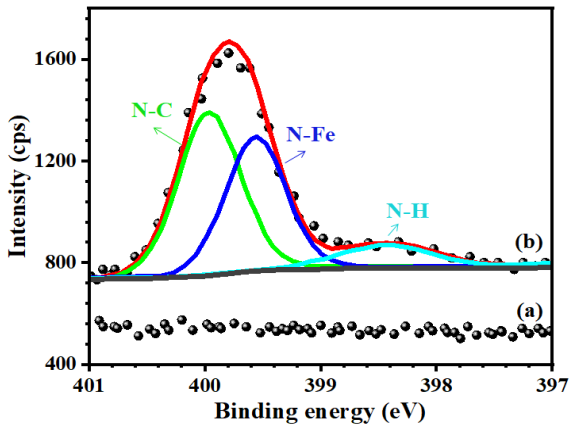

Figure 9: N 1s high resolution peaks for the MS samples immersed in (a) blank and (b) inhibited (0.5 M HCl +400 ppm 1-ABT) solutions.

The N 1s spectra of the coupon immersed in the 1-ABT solution can be divided into three distinct peaks at 399.7±0.1, 399.5±0.1, and 398.4±0.1 eV, which correspond to N-C, N-Fe, and N-H bonds, respectively [49, 50]. As expected, no peaks indicating the presence of nitrogen are observed in the blank solution. So, the XPS results do agree with the gravimetric and electrochemical findings.

3.9. Theoretical investigations

Quantum chemical computations were conducted to examine the impact of electronic parameters and molecular structures on the inhibitory properties of the investigated inhibitors. The optimized molecular structures and the arrangement of key molecular orbitals (HOMO and LUMO) are illustrated in Figure 10. Additionally, Table 6 provides a comprehensive overview of various quantum chemical parameters such as E_{HOMO}, E_{LUMO}, ΔE, χ, μ, ΔN, and η. The ΔE parameter provides insights into the strength of stability of an inhibitor, with smaller values indicating a higher tendency for the compound to be adsorbed on the surface. Increasing values of χ indicate an enhanced propensity to form covalent bonds and fill iron vacant d-orbitals. In the case of μ, when the value exceeds the dipole moment of water (1.85 debye), it signifies a greater inclination of the inhibitor to displace pre-adsorbed water molecules and adsorb onto the steel surface. The electron-donating capacity of a corrosion inhibitor, and consequently its inhibition performance, is enhanced within the range of $0 < \Delta N < 3.6$. According to the HSAB theory, Fe atoms function as soft acids, and molecules with higher softness (lower η), denoting greater reactivity, readily engage in electron sharing and covalent bonding. In comparison to previously reported drugs [14, 30, 51, 52], 1-ABT exhibits improved quantum chemical parameters. Figure 11 displays the low-energy adsorption arrangement of 1-ABT molecules on the Fe (1 1 0) surface. When viewed from the side, the 1-ABT configuration is parallel to the Fe surface, exhibiting minimal distortion. In this configuration, the heteroatoms, particularly N, are in close proximity to the surface. Furthermore, the flat orientation facilitates maximum contact and surface coverage, ensuring an optimal interaction between the inhibitor and the steel system. The $E_{adsorption}$ is -102.254 kcal/mol, with the negative sign indicating a spontaneous adsorption process.

Table 6: Quantum chemical parameters of 1-ABT corrosion inhibitor.

E_{HOMO} (eV)	E_{LUMO} (eV)	ΔE_{gap} (eV)	μ (Debye)	ΔN	η
-5.598	-3.117	2.481	7.4515	1.065	1.2405

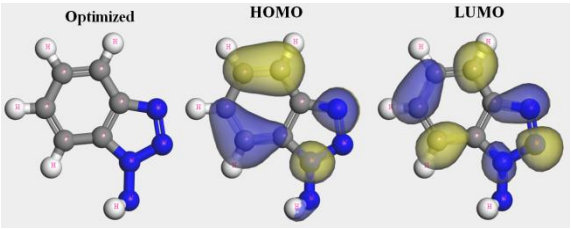

Figure 10: Optimized molecular structure, HOMO and LUMO distribution of the 1-ABT molecule.

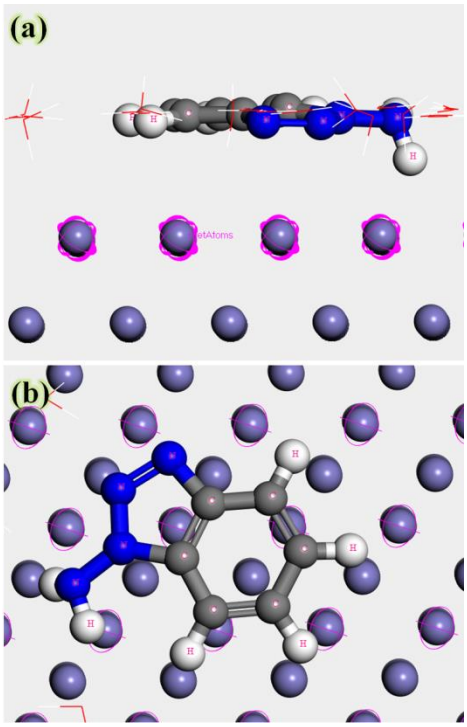

Figure 11: Configuration of adsorbed 1-ABT on Fe (1 1 0): (a) side view, (b) top view.

4. Conclusions

The present study yields the following comprehensive findings:

(i) The 1-ABT drug demonstrates promising potential as a corrosion inhibitor for MS in a 0.5 M HCl environment. The *IE* shows an increase with higher inhibitor concentrations, peaking at approximately 98 % at 400 ppm of 1-ABT. Furthermore, the *IE* values exhibit a notable decline with increasing temperature.

(ii) PDP measurements indicate that 1-ABT acts as a mixed-type corrosion inhibitor, affecting both the dissolution of Fe and the evolution of hydrogen. Moreover, EIS results reveal that the C_{dl} decreases while the R_p increases with rising concentrations of 1-ABT. This suggests a decrease in the local dielectric constant or an increase in the thickness of the electrical double layer due to the adsorption of 1-ABT molecules and the formation of a protective film.

(iii) Thermodynamic calculations demonstrate that the adsorption mechanism of 1-ABT in 0.5 M HCl follows physiochemisorption principles.

(iv) SEM examinations confirm that the presence of 1-ABT reduces the corrosion rate of MS in 0.5 M HCl. This is further supported by XPS results, which verify the adsorption of 1-ABT molecules through nitrogen atoms. Besides, theoretical investigations confirm that nitrogen atoms within 1-ABT molecules offer ideal sites for adsorption on the MS surface.

Based on the effectiveness of 1-ABT in mitigating steel corrosion in HCl media, this study opens up new possibilities for its application beyond its traditional use as a drug. Specifically, 1-ABT can be effectively utilized in various industries, particularly when it is nearing its expiry date as a drug.

5. References

1. Loganathan KT, Thimmakondu VS, Nagarajan S, Natarajan R. Corrosion inhibitive evaluation and DFT studies of 2-(Furan-2-yl)-4, 5-diphenyl-1H-imidazole on mild steel at 1.0 M HCl. J Indian Chem Soc. 2021; 98(9): 100121. https://doi.org/10.1016/j.jics.2021.100121.
2. Motawea MM, Melhi S. Electrochemical and computational studies of an expired vilazodone Drug as environmentally safe corrosion inhibitor for aluminum in chloride medium. J Indian Chem Soc. 2023; 100(6): 101013. https://doi.org/10.1016/j.jics.2023.101013.
3. Salem AM, Wahba AM, El Hossiany A, Fouda AS. Experimental and computational chemical studies on

the corrosion inhibitive properties of metamizole sodium pharmaceutical drug compound for CS in hydrochloric acid solutions. J Indian Chem Soc. 2022; 99(12): 100778. https://doi.org/10.1016/j.jics.2022.100778.
4. Mehta RK, Gupta SK, Yadav M. Synthesized novel carbon dots as green corrosion inhibitor for mild steel in hydrochloric acid: Gravimetric, electrochemical and morphological studies. Diam Relat Mater. 2023; 136: 109992. https://doi.org/10.1016/j.diamond.2023.109992.
5. Bousba S, Allal H, Damous M, Maza S. Computational DFT analysis and molecular modeling on imidazole derivatives used as corrosion inhibitors for aluminum in acidic media. Comput Theor Chem. 2023; 1225: 114168. https://doi.org/10.1016/j.comptc.2023.114168.
6. Souza L, Pereira E, Matlakhova L, Nicolin VAF, Monteiro SN, de Azevedo ARG. ionic liquids as corrosion inhibitors for carbon steel protection in hydrochloric acid solution: a first review. J Mater Res Technol. 2022; 22: 2186-205. https://doi.org/10.1016/j.jmrt.2022.12.066.
7. Mohamed MG, Mahdy A, Obaid RJ, Hegazy MA, Kuo S-W, Aly KI. Synthesis and characterization of polybenzoxazine/clay hybrid nanocomposites for UV light shielding and anti-corrosion coatings on mild steel. J Polym Res. 2021; 28: 1-15. https://doi.org/10.1007/s10965-021-02657-0.
8. Aly KI, Mohamed MG, Younis O, Mahross MH, Abdel-Hakim M, Sayed MM. Salicylaldehyde azine-functionalized polybenzoxazine: Synthesis, characterization, and its nanocomposites as coatings for inhibiting the mild steel corrosion. Prog Org Coat. 2020;138: 105385.https://doi.org/10.1016/ j.porgcoat. 2019. 105385.
9. Mohamed MG, Kuo SW, Mahdy A, Ghayd IM, Aly KI. Bisbenzylidene cyclopentanone and cyclohexanone-functionalized polybenzoxazine nanocomposites: Synthesis, characterization, and use for corrosion protection on mild steel. Mater Today Commun. 2020; 25: 101418. https://doi.org/10.1016/j.mtcomm.2020.101418.
10. Wang Q, Peng Y, Fu S, Yang X, Sun Q, Wang X, et al. Experimental and theoretical investigations of 1, 1'-Dibenzyl-[4, 4'-bipyridine]-1, 1'-diium chloride as effective corrosion inhibitor for Q235 steel in 1 M HCl. Mater Today Commun. 2023; 35: 106169. https://doi.org/10.1016/j.mtcomm.2023.106169.
11. Benhiba F, Benzekri Z, Kerroum Y, Timoudan N, Hsissou R, Guenbour A, et al. Assessment of inhibitory behavior of ethyl 5-cyano-4-(furan-2-yl)-2-methyl-6-oxo-1, 4, 5, 6-tetrahydropyridine-3-carboxylate as a corrosion inhibitor for carbon steel in molar HCl: Theoretical approaches and experimental investigation. J Indian Chem Soc. 2023; 100(2): 100916. https://doi.org/10.1016/j.jics.2023.100916.
12. Zhu Y, Sun Q, Wang Y, Tang J, Wang Y, Wang H. Molecular dynamic simulation and experimental investigation on the synergistic mechanism and synergistic effect of oleic acid imidazoline and l-cysteine corrosion inhibitors. Corr Sci. 2021; 185: 109414. https://doi.org/10.1016/j.corsci.2021.109414.
13. Ziouani A, Atia S, Hamani H, Douadi T, Al-Noaimi M, Gherraf N. Molecular dynamic simulation and experimental investigation on the synergistic mechanism and synergistic effect of (1Z) N [2 (methylthio) phenyl] 2oxopropanehydrazonoyl chloride (S1) corrosion inhibitor on mild steel in acid medium1M HCl. J Indian Chem Soc. 2023; 100(1): 100832. https://doi.org/10.1016/j.jics.2022.100832.
14. Njoku CN, Enendu BN, Okechukwu SJ, Igboko N, Anyikwa SO, Ikeuba AI, et al. Review on anti-corrosion properties of expired antihypertensive drugs as benign corrosion inhibitors for metallic materials in various environments. Results Eng. 2023; 18: 101183. https://doi.org/10.1016/j.rineng.2023.101183.
15. Chen Y, Hu Y, Ding C, Ni Q, Jiang Y, Zhao J, et al. The corrosion behaviors of carbon steel under the effect of AC and imidazoline quaternary ammonium salt corrosion inhibitor. Int J Electrochem Sci. 2023; 18(6): 100143. https://doi.org/10.1016/j.ijoes.2023.100143.
16. Liu E-B, Tang H, Zhang Y-H, Li D-J, Kou B, Liu N, et al. Experiment and numerical simulation of distribution law of water-based corrosion inhibitor in natural gas gathering and transportation pipeline. Pet Sci. 2023; 20: 1857-73. https://doi.org/10.1016/j.petsci.2023.01.015.
17. Liao B, Ma S, Zhang S, Li X, Quan R, Wan S, et al. Fructus cannabis protein extract powder as a green and high effective corrosion inhibitor for Q235 carbon steel in 1 M HCl solution. Int J Biol Macromol. 2023; 239: 124358. https://doi.org/10.1016/j.ijbiomac.2023.124358.
18. Li X, Chen L, Xie B, Lai C, He J, Feng J, et al. Two semi flexible nonplanar double Schiff bases as corrosion inhibitors for mild steel in HCl solution: Experimental and theoretical investigations. J Environ Chem Eng. 2023; 11(3): 110077. https://doi.org/10.1016/j.jece.2023.110077.
19. Anandkumar B, Krishna NG, Solomon RV, Nandakumar T, Philip J. Synergistic enhancement of corrosion protection of carbon steels using corrosion inhibitors and biocides: Molecular adsorption studies, DFT calculations and long-term corrosion performance evaluation. J Environ Chem Eng. 2023; 11(3): 109842. https://doi.org/10.1016/j.jece.2023.109842.
20. Gan P, Zhang D, Gao L, Xin Z, Li X. Inhibitive effect of anionic/zwitterionic hybrid surfactants on the self-corrosion of anode for alkaline Al-air battery. Colloids Surfaces A Physicochem Eng Asp. 2023; 670: 131530. https://doi.org/10.1016/j.colsurfa.2023.131530.
21. Zhang A, Wang Y, Wang H. Preparation of inorganic-polymer nano-emulsion inhibitor for corrosion resistance of steel reinforcement for

concrete. Alexandria Eng J. 2023; 66: 537-42. https://doi.org/10.1016/j.aej.2022.11.020.
22. Huang L, Li H-J, Wu Y-C. Comprehensive evaluation of corrosion inhibition performance and ecotoxicological effect of cinchona IIa as a green corrosion inhibitor for pickling of Q235 steel. J Environ Manage. 2023; 335: 117531. https://doi.org/10.1016/j.jenvman.2023.117531.
23. Al-Amiery A. Gravimetric and Density Functional Theory Investigations on 4-Amioantipyrin Schiff base as an inhibitor for mild steel in HCl solution. Prog Color Colorant Coat. 2023; 16: 255-69. https://doi.org/10.30509/PCCC.2023.167077.1196.
24. Al-Amiery A. Investigation of the Corrosion Inhibition Properties of 4-Cyclohexyl-3-Thiosemicarbazide on Mild Steel in 1 M HCl Solution. Prog Color Colorant Coat. 2023. https://doi.org/10.30509/PCCC.2023.167126.1212.
25. Shojaee S, Zandi MS, Rastakhiz N. The effect of Tetracycline drug as a green corrosion inhibitor for carbon steel in HCl media. J Indian Chem Soc. 2022; 99(10): 100700. https://doi.org/10.1016/j.jics.2022.100700.
26. Kannan MB, Rahuma M, Khakbaz H, Melchers R. Antipsychotic drug waste: A potential corrosion inhibitor for mild steel in the oil and gas industry. Waste Manag. 2022; 145: 38-47. https://doi.org/10.1016/j.wasman.2022.04.029.
27. Zakaria K, Abbas MA, Bedair MA. Herbal expired drug bearing glycosides and polysaccharides moieties as green and cost-effective oilfield corrosion inhibitor: Electrochemical and computational studies. J Mol Liq. 2022; 352: 118689. https://doi.org/10.1016/j.molliq.2022.118689.
28. Gece G. Drugs: A review of promising novel corrosion inhibitors. Corr Sci. 2011; 53(12): 3873-98. https://doi.org/10.1016/j.corsci.2011.08.006.
29. Raja PB, Ismail M, Ghoreishiamiri S, Mirza J, Ismail MC, Kakooei S, et al. Reviews on corrosion inhibitors: a short view. Chem Eng Commun. 2016; 203(9): 1145-56. https://doi.org/10.1080/00986445.2016.1172485.
30. Fayomi OSI, Akande IG, Nsikak U. An overview of corrosion inhibition using green and drug inhibitors. In: Journal of Physics: Conference Series. IOP Publishing; 2019. p. 22022. https://doi.org/10.1088/1742-6596/1378/2/022022.
31. Campbell CD, Rees CW. Reactive intermediates. Part I. Synthesis and oxidation of 1-and 2-aminobenzotriazole. J Chem Soc C Org. 1969; (5): 742-7. https://doi.org/10.1039/J39690000742.
32. Pour-Ali S, Kiani-Rashid A, Babakhani A. Improved corrosion inhibition of 3-amino-1, 2, 4-triazole on mild steel electrode in HCl solution using surface nanocrystallization. Int J Mater Res. 2016; 107(11): 1031-40. https://doi.org/10.3139/146.111432.
33. Pour-Ali S, Hejazi S. Tiazofurin drug as a new and non-toxic corrosion inhibitor for mild steel in HCl solution: Experimental and quantum chemical investigations. J Mol Liq. 2022; 354: 118886. https://doi.org/10.1016/j.molliq.2022.118886.
34. McCafferty E. Introduction to corrosion science. Springer Science & Business Media; 2010.
35. Fouda AS, Ismail MA, Al-Khamri AA, Abousalem AS. Experimental, quantum chemical and molecular simulation studies on the action of arylthiophene derivatives as acid corrosion inhibitors. J Mol Liq. 2019; 290: 111178. https://doi.org/10.1016/j.molliq.2019.111178.
36. Iroha NB, Madueke NA, Mkpenie V, Ogunyemi BT, Nnanna LA, Singh S, et al. Experimental, adsorption, quantum chemical and molecular dynamics simulation studies on the corrosion inhibition performance of Vincamine on J55 steel in acidic medium. J Mol Struct. 2021; 1227: 129533. https://doi.org/10.1016/j.molstruc.2020.129533.
37. Kaya S, Guo L, Kaya C, Tüzün B, Obot IB, Touir R, et al. Quantum chemical and molecular dynamic simulation studies for the prediction of inhibition efficiencies of some piperidine derivatives on the corrosion of iron. J Taiwan Inst Chem Eng. 2016; 65: 522-9. https://doi.org/10.1016/j.jtice.2016.05.034 .
38. Yuan X, Luo K, Zhang K, He J, Zhao Y, Yu D. Combinatorial vibration-mode assignment for the FTIR spectrum of crystalline melamine: A strategic approach toward theoretical IR vibrational calculations of triazine-based compounds. J Phys Chem A. 2016; 120(38): 7427-33. https://doi.org/10.1021/acs.jpca.6b06015.
39. Wang Z, Lv P, Hu Y, Hu K. Thermal degradation study of intumescent flame retardants by TG and FTIR: Melamine phosphate and its mixture with pentaerythritol. J Anal Appl Pyrolysis. 2009; 86(1): 207-14. https://doi.org/10.1016/j.jaap.2009.06.007.
40. Zeng Y, Kang L, Wu Y, Wan S, Liao B, Li N, et al. Melamine modified carbon dots as high effective corrosion inhibitor for Q235 carbon steel in neutral 3.5 wt% NaCl solution. J Mol Liq. 2022; 349: 118108. https://doi.org/10.1016/j.molliq.2021.118108.
41. Zhu H, Li X, Lu X, Wang J, Hu Z, Ma X. Efficiency of Gemini surfactant containing semi-rigid spacer as microbial corrosion inhibitor for carbon steel in simulated seawater. Bioelectrochem. 2021; 140: 107809. https://doi.org/10.1016/j.bioelechem.2021.107809.
42. Finšgar M, Jackson J. Application of corrosion inhibitors for steels in acidic media for the oil and gas industry: A review. Corr Sci. 2014; 86: 17-41. https://doi.org/10.1016/j.corsci.2014.04.044.
43. Ganjoo R, Sharma S, Thakur A, Assad H, Sharma PK, Dagdag O, et al. Experimental and theoretical study of sodium cocoyl glycinate as corrosion inhibitor for mild steel in hydrochloric acid medium. J Mol Liq. 2022; 364: 119988. https://doi.org/10.1016/j.molliq.2022.119988.
44. Kosari A, Momeni M, Parvizi R, Zakeri M, Moayed MH, Davoodi A, et al. Theoretical and electrochemical assessment of inhibitive behavior of

some thiophenol derivatives on mild steel in HCl. Corr Sci. 2011; 53(10): 3058-67. https://doi.org/10.1016/j.corsci.2011.05.009.
45. Aljourani J, Raeissi K, Golozar MA. Benzimidazole and its derivatives as corrosion inhibitors for mild steel in 1M HCl solution. Corr Sci. 2009; 51(8): 1836-43. https://doi.org/10.1016/j.corsci.2009.05.011.
46. Saranya J, Sowmiya M, Sounthari P, Parameswari K, Chitra S, Senthilkumar K. N-heterocycles as corrosion inhibitors for mild steel in acid medium. J Mol Liq. 2016; 216:42-52. https://doi.org/10.1016/j.molliq.2015.12.096.
47. Bahron H, Ghani AA, Embong Z, Alharthi AI, Harun MK, Alias Y. Adsorption, electrochemistry, DFT and inhibitive effect of imines derived from tribulin on corrosion of mild steel in 1 M HCl. J Mol Struct. 2021; 1235: 130206. https://doi.org/10.1016/j.molstruc. 2021.130206.
48. Verma C, Rhee KY, Quraishi MA, Ebenso EE. Pyridine based N-heterocyclic compounds as aqueous phase corrosion inhibitors: A review. J Taiwan Inst Chem. Eng. 2020; 117: 265-77. https://doi.org/10.1016/j.jtice.2020.12.011.
49. Singh P, Srivastava V, Quraishi MA. Novel quinoline derivatives as green corrosion inhibitors for mild steel in acidic medium: electrochemical, SEM, AFM, and XPS studies. J Mol Liq. 2016; 216: 164-73. https://doi.org/10.1016/j.molliq.2015.12.086.
50. Zhang W, Li H-J, Wang M, Wang L-J, Pan Q, Ji X, et al. Tetrahydroacridines as corrosion inhibitor for X80 steel corrosion in simulated acidic oilfield water. J Mol Liq. 2019; 293: 111478. https://doi.org/10.1016/j.molliq.2019.111478.
51. Vengatesh G, Karthik G, Sundaravadivelu M. A comprehensive study of ondansetron hydrochloride drug as a green corrosion inhibitor for mild steel in 1 M HCl medium. Egypt J Pet. 2017; 26(3): 705-19. https://doi.org/10.1016/j.ejpe.2016.10.011.

How to cite this article:
Namdar-Asl H, Fakheri F, Pour-Ali1 S, Tavangar R, Hejazi S. Synthesis and Corrosion Inhibition Study of 1-aminobenzotriazole for Mild Steel in HCl Solution: Electrochemical, Surface Analysis, and Theoretical Investigations. Prog Color Colorants Coat. 2024;17(1):61-74. Doi: 10.30509/pccc.2023.167145.1224